JACS
JOURNAL OF THE AMERICAN CHEMICAL SOCIETY

Article

pubs.acs.org/JACS

Modeling Ti/Ge Distribution in $LiTi_{2-x}Ge_x(PO_4)_3$ NASICON Series by ^{31}P MAS NMR and First-Principles DFT Calculations

Virginia Diez-Gómez,* Kamel Arbi,† and Jesús Sanz

Instituto de Ciencia de Materiales de Madrid, Consejo Superior de Investigaciones Científicas (ICMM-CSIC), Sor Juana Inés de la Cruz, 3, 28049 Madrid, Spain

Supporting Information

ABSTRACT: Ti/Ge distribution in rhombohedral $LiTi_{2-x}Ge_x(PO_4)_3$ NASICON series has been analyzed by ^{31}P magic-angle spinning nuclear magnetic resonance (MAS NMR) spectroscopy and first-principles density functional theory (DFT) calculations. Nuclear magnetic resonance is an excellent probe to follow Ti/Ge disorder, as it is sensitive to the atomic scale environment without long-range periodicity requirements. In the samples considered here, PO_4 units are surrounded by four Ti/Ge octahedra, and then, five different components ascribed to $P(OTi)_4$, $P(OTi)_3(OGe)$, $P(OTi)_2(OGe)_2$, $P(OTi)(OGe)_3$, and $P(OGe)_4$ environments are expected in ^{31}P MAS NMR spectra of $R\bar{3}c$ NASICON samples. However, ^{31}P MAS NMR spectra of analyzed series display a higher number of signals, suggesting that, although the overall symmetry remains $R\bar{3}c$, partial substitution causes a local decrement in symmetry. With the aid of first-principles DFT calculations, 10 detected ^{31}P NMR signals have been assigned to different $Ti_{4-n}Ge_n$ arrangements in the $R3$ subgroup symmetry. In this assignment, the influence of octahedra of the same or different $R_2(PO_4)_3$ structural units has been considered. The influence of bond distances, angles and atom charges on ^{31}P NMR chemical shieldings has been discussed. Simulation of the $LiTi_{2-x}Ge_x(PO_4)_3$ series suggests that detection of 10 P environments is mainly due to the existence of two oxygen types, O1 and O2, whose charges are differently affected by Ge and Ti occupation of octahedra. From the quantitative analysis of detected components, a random Ti/Ge distribution has been deduced in next nearest neighbor (NNN) sites that surround tetrahedral PO_4 units. This random distribution was supported by XRD data displaying Vegard's law.

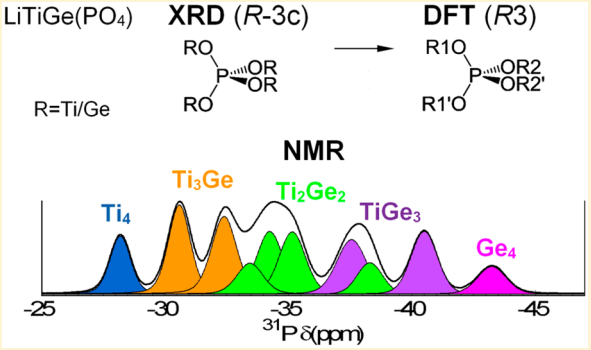

INTRODUCTION

In the past decades, lithium-ion conducting solids have been investigated for potential applications as electrolytes in all-solid state lithium batteries.[1−4] For that, high lithium mobility and electrochemical stability are required. Most lithium ion conductors, such as Li_3N, Li-β alumina, lithium lanthanum titanates ($Li_{3x}La_{(2/3)-x}TiO_3$), LISICON ($Li_{2+2x}Zn_{1-x}GeO_4$), LIPON ($xLi_2O-yP_2O_5-zPON$), and lithium sulfide glasses ($Li_2S-P_2O_5-LiI$ and $Li_2S-SiS_2-Li_3PO_4$), have either high ionic conductivity or high electrochemical stability but rarely both.[4−10] In the case of $LiR_2(PO_4)_3$, Li NASICON compounds have received much attention because of their high ionic conductivity and stability against moisture.[3,9,11−13]

The NASICON $LiR_2(PO_4)_3$ framework is built up by $R_2(PO_4)_3$ units, where two RO_6 octahedra share oxygens with three PO_4 tetrahedra. Tetrahedra and octahedra of contiguous $R_2(PO_4)_3$ units are bounded to form the three-dimensional network of NASICON structure (Figure 1). In this network, each octahedron is connected to six tetrahedra and each tetrahedron to four octahedra. Symmetry of $LiR_2(PO_4)_3$ compounds is usually rhombohedral $R\bar{3}c$, although in some cases a triclinic distortion (space group $C\bar{1}$) was detected.[14−18] In rhombohedral samples, Li^+ ions occupy M1 sites surrounded by six oxygen atoms,[14,15] but in triclinic phases, Li^+ ions are at intermediate sites M12, coordinated to four oxygen atoms between M1 and M2 positions.[16−18] In sodium $NaR_2(PO_4)_3$

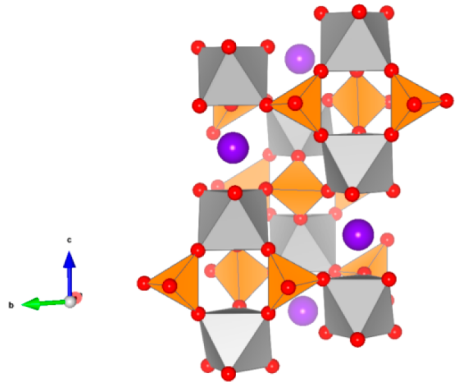

Figure 1. Detail of NASICON structure with R octahedra denoted in gray, P tetrahedra in orange, O atoms in red, and Li atoms in purple.

Received: April 7, 2016
Published: July 2, 2016

DOI: 10.1021/jacs.6b03583
J. Am. Chem. Soc. 2016, 138, 9479−9486

homologues, bigger Na cations only occupy M1 sites at ternary axes.[19] In $Li_{1+x}R^{IV}_{2-x}S_x^{III}(PO_4)_3$ series, with R = Ti, Zr, Hf, Ge, and Sn and S = Al, Ga, and In, the increment detected in Li conductivity has been ascribed to the occupation of M3 (located in M2 cavities) at the expenses of M1 sites.[20−24]

In order to understand physical and chemical properties of NASICON compounds, a detailed knowledge of the local structure and cation order/disorder is required. Solid-state nuclear magnetic resonance (SS-NMR) can be used to study local atomic arrangements without long-range order. Subtle differences in local environment produce changes on chemical shielding, achieving, in some cases, enough resolution to differentiate MAS NMR components. In the case of NASICON $LiR_2(PO_4)_3$ materials, each P tetrahedra is surrounded by four octahedra, which permits one to follow the main features of octahedral cation distribution around P atoms.

Density functional theory (DFT) calculations can be used to analyze the influence of next nearest neighbor (NNN) sites on the chemical shift of atoms.[25] The comparison between experimental NMR and DFT-calculated parameters has previously allowed the assessment of atomic arrangements, where diffraction data were not conclusive.[26,27] Optimization of structural parameters makes possible a better analysis of electronic arrangement in chemical bonds.[28,29] In particular, the influence of bond angles and lengths on ^{31}P NMR chemical shielding has been previously tested with DFT techniques.[30−32]

The aim of the present work is the analysis of the Ti/Ge distribution in the $LiTi_{2-x}Ge_x(PO_4)_3$ series using ^{31}P MAS NMR spectroscopy. For a better understanding of deduced parameters, a parallel NMR and DFT study of this series has been performed and the assignment of experimental signals to specific environments done. With the aid of DFT, the sensitivity of NMR chemical shift to atom charges, bond distances, and bond angles has been investigated. The quantitative analysis of ^{31}P NMR spectra has been used to deduce the main characteristics of the Ti/Ge distribution.

EXPERIMENTAL SECTION

Samples. $LiTi_{2-x}Ge_x(PO_4)_3$ samples, with $0 \le x \le 2$, were prepared by the ceramic route. Stoichiometric amounts of Li_2CO_3, TiO_2/GeO_2, and $(NH_4)_2HPO_4$ were first dried at 393 K for 10 h and then mixed in a platinum crucible and heated at increasing temperatures as described elsewhere.[21,33] After each treatment, the mixture was ground in an agate mortar and analyzed by X-ray diffraction to assess the formation of single phases of prepared compounds. Samples were stored for later use when characteristic peaks of NASICON phases were detected and those of reagents or intermediate pyrophosphates eliminated from XRD patterns.

Techniques. XRD powder patterns were recorded with the Cu Kα radiation (λ = 1.540598 Å) in the 10−70° 2θ range with a step size of 0.02° and a counting time of 0.1 s·step^{-1} in a PW 1050/25 Phillips diffractometer. Unit cell parameters of formed phases were deduced by using the Fullprof program[34] (pattern matching technique).

^{31}P NMR spectra were recorded at room temperature in an AVANCE Bruker spectrometer (9.4 T). The frequency used was 161.97 MHz. NMR signals were obtained after $\pi/2$ pulse irradiation (3.5 μs) with a recycling time of 600 s (single pulse experiments). The number of scans was 16. To improve the experimental resolution, samples were spun at 10 kHz around an axis inclined 54°44′ with respect to the external magnetic field (MAS technique) during spectra recording. ^{31}P chemical shifts were referred to an 85% H_3PO_4 aqueous solution. The fitting of NMR spectra was performed with the DMFIT software package.[35]

DFT Simulations. Calculations were carried out using the CASTEP 7.0 code.[36] In this work, density functional theory (DFT), which employs the gauge including projector augmented wave (GIPAW)[37] algorithm, enabled the reconstruction of all-electron wave functions in the presence of a magnetic field. The generalized gradient approximation (GGA) PBE[38] functional was used, and the core−valence interactions were described with ultrasoft reported pseudopotentials.[39] Structural parameters (unit cell and atomic positions) reported in ICSD 95979[40] (for Ti) and 69763[14] (for Ge) were used in DFT calculations.

Crystal structures were reproduced by using periodic boundary conditions. For geometrical optimization and NMR parameter calculation, numerical integrals were performed over the Brillouin zone, using a Monkhorst−Pack grid with a k-point spacing of 0.04 Å^{-1}. Wave functions were expanded in plane waves with kinetic energy smaller than the cutoff energy, 1200 eV. With the chosen kinetic energy cutoff and k-point grid, the total energy converged to $\ll 1 \times 10^{-4}$ eV·atom^{-1}, atomic forces to $\ll 1 \times 10^{-2}$ eV·Å^{-1}, and ^{31}P chemical shifts to <0.1 ppm. The optimization of geometry parameters was performed allowing atomic coordinates and cell constants to vary. Optimizations were pursued until the energy difference, maximum atomic forces, maximum atomic displacements, and maximum stress tensor components felt below 5×10^{-6} eV·atom^{-1}, 1×10^{-2} eV·Å^{-1}, 5×10^{-4} Å, and 2×10^{-2} GPa tolerances.

NMR shielding tensors, **R**, were deduced from structural calculations, for that, isotropic shielding values, σ_{iso}, were calculated as (1/3) Tr{**R**}. To correlate experimental to calculated parameters, a previous DFT calculation was performed in four reported magnesium phosphates with different degrees of condensation (see section S1 of the Supporting Information). A least mean square regression was used to obtain the equation $\delta_{iso} = -0.8618 \times \sigma_{iso} + 237.7$, with $R^2 = 0.9995$ (RMSE = 0.4178) which correlates experimental isotropic chemical shifts to calculated isotropic chemical shieldings for reference compounds. This equation was afterward used to reference chemical shieldings deduced in $LiTi_{2-x}Ge_x(PO_4)_3$ samples.

RESULTS AND DISCUSSION

XRD Analysis. XRD patterns of $LiTi_{2-x}Ge_x(PO_4)_3$ series ($0 \le x \le 2$), recorded at room temperature, are given in Figure 2a. In all cases, samples display $R\bar{3}c$ rhombohedral symmetry.

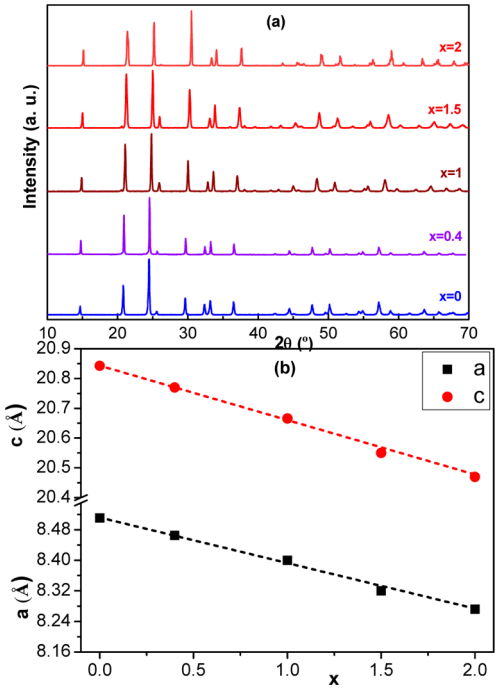

Figure 2. (a) XRD patterns and (b) dependence of unit-cell parameters on the $LiTi_{2-x}Ge_x(PO_4)_3$ sample composition.

DOI: 10.1021/jacs.6b03583
J. Am. Chem. Soc. 2016, 138, 9479−9486

Diffraction peaks are shifted to higher 2θ values when Ti (r_i = 0.61 Å) is substituted by Ge (r_i = 0.53 Å) cations. The plot of unit-cell parameters shows the linear **a** and **c** decrease with Ge content (Figure 2b). The linear variation of unit-cell parameters has often been related to the random distribution of cations in solid solutions (Vegard's law).[41]

^{31}P MAS NMR Study. In $LiR_2(PO4)_3$ $R\bar{3}c$ structures, Li atoms occupy 6b, P atoms 18e, R(Ge/Ti) atoms 12c, and O1 and O2 atoms 36f Wickoff sites. In agreement with structural information, ^{31}P MAS NMR spectra of $LiGe_2(PO_4)_3$ and $LiTi_2(PO_4)_3$ are formed by a single component ascribed to $P(OGe)_4$ and $P(OTi)_4$ environments. The difference on chemical shift values, from −27.7 to −43.7 ppm, has been associated with distinct polarization strength (q/r) of Ge and Ti cations.

^{31}P MAS NMR spectra of the analyzed $LiTi_{2-x}Ge_x(PO_4)_3$ series are depicted in Figure 3, where detected peaks shift upfield as a consequence of Ge for Ti substitution. For Ti richer samples, signals appear in the range between −27.7 and −35 ppm, while, for Ge rich samples, signals appear in the range between −35 and −43.7 ppm. For intermediate compositions, signals appear in the range between −27.7 and −43.7 ppm. The line width of signals in intermediate compositions is much broader than that in pure phases.

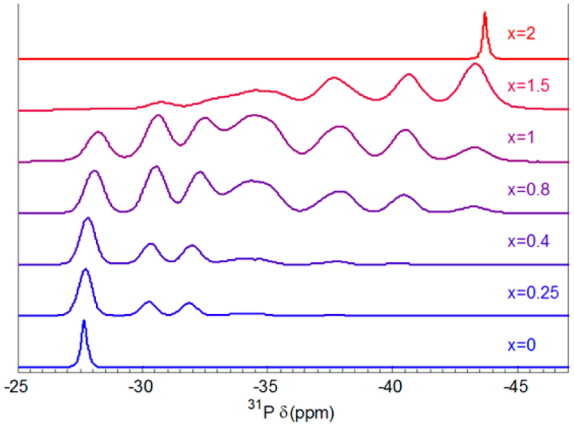

Figure 3. ^{31}P MAS NMR spectra along the $LiTi_{2-x}Ge_x(PO_4)_3$ series, in which each component corresponds to a different octahedral environment of P tetrahedra (see text).

In previous works, the presence of five equally spaced ^{31}P MAS NMR components has been associated with $P(OR)_4$, $P(OR)_3(OR')$, $P(OR)_2(OR')_2$, $P(OR)$ $(OR')_3$, and $P(OR')_4$ environments, in samples where two different cations occupy four equivalent octahedral sites that surround PO_4 units.[42−44] In NASICON samples with $R\bar{3}c$ symmetry, relative intensities of five detected bands should follow the expression a^4, $4a^3b$, $6a^2b^2$, $4ab^3$, b^4, where a and b stand for the relative occupation of octahedral sites by two cations.[45] In $LiTi_{2-x}Ge_x(PO_4)_3$ series, however, the amount of detected peaks is considerably higher. The deconvolution of ^{31}P MAS NMR spectra with Gaussian components required the presence of at least 10 components to reproduce experimental envelopes. In this analysis, the line width of components increases as the concentration of Ge increases.

A higher number of components could be caused by the formation of different phases in analyzed compounds; however, the presence of different phases was not confirmed in XRD patterns. A global decrement of the symmetry could also produce the splitting of ^{31}P NMR signals, but XRD patterns do not support this hypothesis. Finally, the occupation of octahedral sites by two different cations could also decrease the local symmetry at P sites. In this case, a maximum of 2^4 = 16 arrangements could ideally be detected by NMR if four different octahedral sites were partially occupied by two cations.

DFT Calculations. One way to simulate materials with density functional theory is the use of the cluster approach; however, cluster size or charge neutrality at the cluster edge are difficult to define. On the other hand, a periodic approach does not have the mentioned difficulties, offering the advantage of calculating NMR parameters of all sites within a single calculation. In the present work, the last methodology has been adopted.

To simulate disordered materials under periodic boundary conditions, elimination of symmetry elements in the unit cell (and in some cases generation of a supercell) has been used to recreate a higher variety of environments.[46−48] In order to maintain geometrical restrictions deduced by XRD structural refinements, different subgroups of $R\bar{3}c$ have been considered to describe octahedral cation arrangements. In Figure 4, subgroups relating $R\bar{3}c$ and $R3$ S.G. are analyzed. The consideration of these subgroups reduces the calculation time in comparison with that required by triclinic S.G.

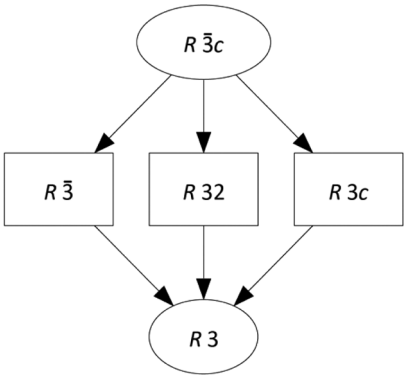

Figure 4. Group−subgroup graph relating $R\bar{3}c$ and $R3$ S.G.

When symmetry is decreased preserving unit-cell volume, Wickoff positions of the $R\bar{3}c$ S.G. undergo the splittings given in Table 1. The analysis of this table shows that, when going from $R\bar{3}c$ to $R\bar{3}$ or $R3c$, the number of octahedral sites is doubled, and when going to $R32$, the number of tetrahedral sites is also doubled. Finally, when symmetry decreases to $R3$, the number of tetrahedral sites is doubled and the number of octahedral sites is quadrupled compared to the parent $R\bar{3}c$ S.G. (see Table 1).

Table 1. Splittings of Wickoff Positions for Different Subgroups of the Parent $R\bar{3}c$ S.G.

	$R\bar{3}c$	$R\bar{3}$	$R32$	$R3c$	$R3$
R	12c	6c, 6c	6c, 6c	6a, 6a	3a, 3a, 3a, 3a
P	18e	18f	9d, 9e	18b	9b, 9b
O1	36f	18f, 18f	18f, 18f	18f, 18f	9b, 9b, 9b, 9b
O2	36f	18f, 18f	18f, 18f	18f, 18f	9b, 9b, 9b, 9b
Li	6b	3a, 3b	6c	6a	3a, 3a

From the crystallographic point of view, the widest variety of octahedral arrangements around a P atom can be described

DOI: 10.1021/jacs.6b03583
J. Am. Chem. Soc. 2016, 138, 9479−9486

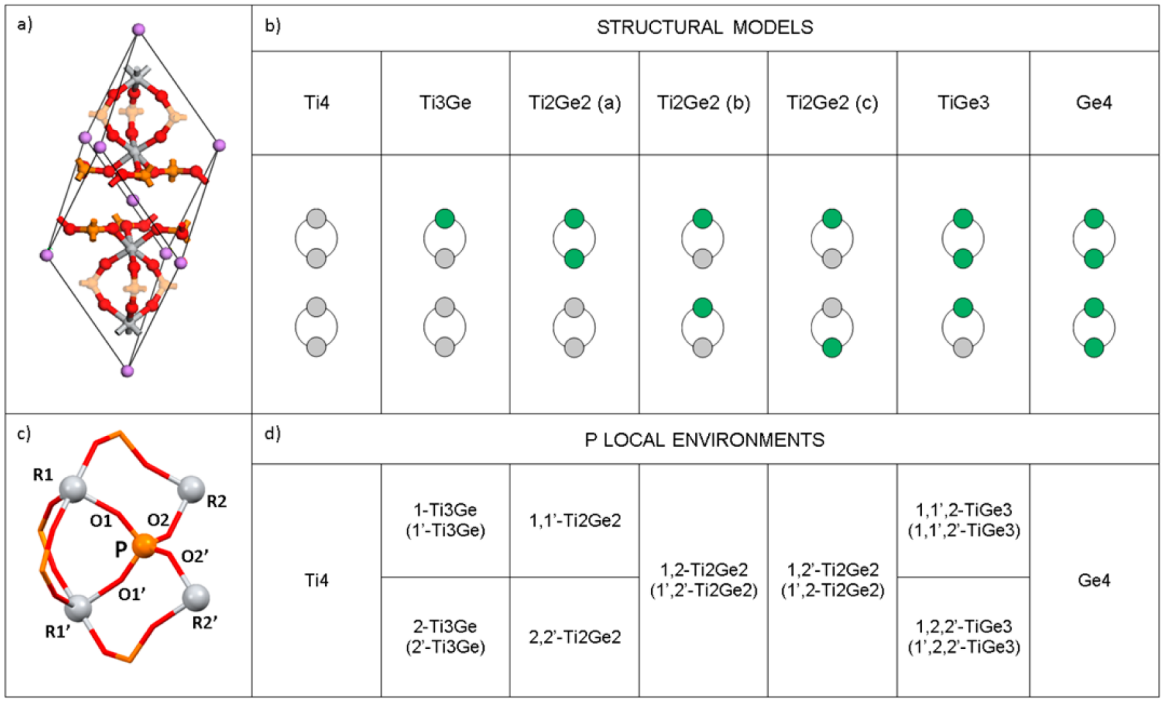

Figure 5. (a) Rhombohedral unit cell used in calculations. (b) Schematic representation of different structural models. (c) P atom environments (R1 and R1′ cations form part of the same $R_2(PO_4)_3$ unit, and R2 and R2′ form part of different units). (d) Nomenclature used to denote P local environments.

with the *R*3 unit cell. *R*3 is the only S.G. that allows an independent substitution on the four NNN octahedral sites surrounding a given P tetrahedron. In Figure 5a, a rombohedral unit cell representation of the Ti pure compound is shown (R atoms in gray). Six faint P atoms have been added to illustrate the arrangement of $R_2(PO_4)_3$ structural blocks ("lantern"). With variable occupation of four octahedral sites taken into account, seven structural models have been considered in DFT simulations to describe different environments. In Figure 5b, a schematic representation of models is given. The four circles stand for the four R atoms of two lanterns included in the rhombohedral unit cell. Green circles denote substitution of Ti by Ge in different R sites of the two $R_2(PO_4)_3$ units.

In Figure 5c, it is shown how, from the local point of view, crystallographic oxygen atoms O1 and O2 have been differentiated as O1, O1′, O2, and O2′ and four R cations surrounding each P atom are denoted as R1 and R1′ sites of the same $R_2(PO_4)_3$ unit and R2 and R2′ sites of neighboring units. In this work, we have assumed that only the nearest four octahedra that share oxygen atoms with P tetrahedra have an influence on the chemical shielding of P atoms, and cations located further than 4 Å have a limited effect. In this case, some broadening of the NMR components could be produced as a consequence of substitutional disorder outside the considered sphere. With the number of octahedra taken into account, a maximum of 16 environments can be considered around each P site. The nomenclature used to denote different P environments is based on the specification (1, 1′, 2, and 2′) of Ge sites occupation.

In Figure 5d, environments found in each structural model are detailed. With the local arrangement of atoms inside the spheres considered here taken into account, some of the P environments are identical. In section S2 of the Supporting Information, it is shown, as an example, how in model TiGe3 the 1,1′,2′-TiGe3 environment can also be labeled as 1,1′,2-TiGe3 and the 1′,2,2′-TiGe3 environment as 1,2,2′-TiGe3. Because of this, some pairs of environments can be considered as equivalent (one of each pair is written between brackets in Figure 5d and will not be considered in the rest of the manuscript). On the basis of these ideas, only 10 P environments will be discussed.

For Ti4 and Ge4 models, atomic positions and unit-cell parameters of pure $R\bar{3}c$ phases were considered (ICSD structures 95979 and 69763, respectively).[14,40] For the rest of the models, atomic positions were taken from the ICSD structure 95979 and cell parameters were interpolated between those of two Ti and Ge end-members. Atomic coordinates and unit cell parameters of all models were allowed to relax prior to performing NMR parameter calculations. In the *R*3 model, two tetrahedral P sites exist; however, their calculated chemical shift values differ less than 0.02 ppm when the same environment is considered (case of Ti4, Ti2Ge2(b), Ti2Ge2(c), and Ge4). When structures are simulated with higher symmetry than *R*3 (Ti4 in $R\bar{3}c$; Ti2Ge2(a) in *R*32; Ti2Ge2(b) in $R\bar{3}$; Ti2Ge2(c) in *R*3*c*; and Ge4 in $R\bar{3}c$), calculated ^{31}P chemical shifts of considered environments just display lower variations than a couple of tenths of ppm. This confirms the assumption that the nearest four octahedra that share oxygen atoms with P tetrahedra have the main effect on the analyzed chemical shifts of P atoms.

In the case of 1/4 substitution (Ti3Ge model in Figure 5b), environments 1-Ti3Ge and 2-Ti3Ge are present, while, in 3/4 substitution (TiGe3 model), 1,1′,2-TiGe3 and 1,2,2′-TiGe3 environments are differentiated. Two pairs of detected bands in ^{31}P MAS NMR spectra can be assigned to these two pairs of environments, indicating that R1 and R2 octahedral sites are different. The intensity of the signals of each pair is the same in

DOI: 10.1021/jacs.6b03583
J. Am. Chem. Soc. 2016, 138, 9479−9486

all analyzed compositions, showing that Ti or Ge cations do not display any preference for sites denoted as 1 and 2.

For 1/2 substitution, three different Ti2Ge2 models are considered (third, fourth, and fifth columns of Figure 5b) whose P atoms are surrounded by (a) 1,1′-Ti2Ge2 and 2,2′-Ti2Ge2 environments, (b) 1,2-Ti2Ge2 environment, and (c) 1,2′-Ti2Ge2 environment.

If R1 ≠ R1′ ≠ R2 ≠ R2′ is assumed, six different Ti2Ge2 signals could be detected in ^{31}P MAS NMR spectra; however, if R1 = R1′ and R2 = R2′, three Ti2Ge2 signals should be detected (environments on fourth and fifth columns of Figure 5d would be identical). A third option is, once a substitution is made in position R1 or R1′, if two external R2 and R2′ sites are differentiated, four detected components should be resolved (R1 = R1′ and R2 ≠ R2′). In the same way, a substitution in position R2 or R2′ could also differentiate R1 and R1′ sites (R2 = R2′ and R1 ≠ R1′). Calculated and experimental chemical shift values show four different environments for Ti2Ge2 arrangements around a P atom, suggesting that the last model is operative and interaction between two types of structural sites must be invoked.

The chemical shifts for 10 considered environments were calculated with DFT techniques; resulting values are summarized in section S3 of the Supporting Information and depicted in Figure 6.

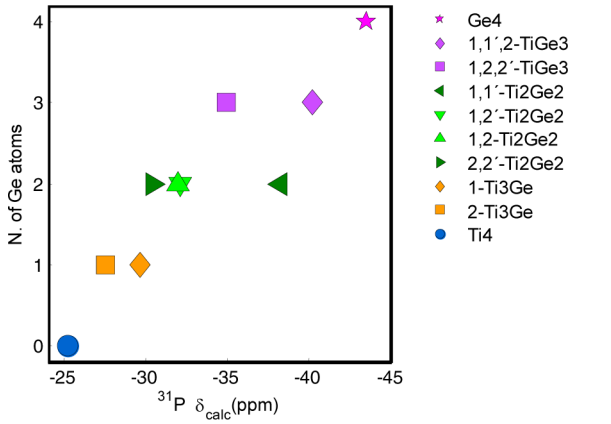

Figure 6. Calculated ^{31}P chemical shift values as a function of the number of Ge in NNN octahedral positions.

Figure 6 shows that substitution of Ti by Ge in position 1 causes more negative shifts than that in position 2 (orange symbols). The nonequivalence of inner and outer octahedral sites of the lantern seems to be the main cause for the splitting of bands compared to five-component patterns in ^{31}P NMR spectra. The calculated chemical shift for the 1,1′-Ti2Ge2 environment is much more negative than that for the 1,2-Ti2Ge2, 1,2′-Ti2Ge2, and 2,2′-Ti2Ge2 environments (green symbols in Figure 6), indicating that the substitution in contiguous sites of the same lantern has a much bigger effect than that in external units.

In Figure 6, it can be seen that the consecutive substitution of Ti by Ge in positions 2 and 2′ changes chemical shift in a linear way, but in the case of the substitution in the 1 and 1′ positions, the second substitution has a bigger effect than the first one. Observed chemical shift values for 1,2-Ti2Ge2 and 1,2′-Ti2Ge2 environments show a greater difference than that calculated by DFT.

All ^{31}P MAS NMR spectra were deconvoluted in 10 components. Each detected component was assigned according to chemical shifts obtained in DFT calculations (Figure 7). The agreement between calculated and experimental chemical shifts is quite good (see section S3 of the Supporting Information). It is worth noting that Ti4 and Ge4 NMR components are thinner in pure phases than in intermediate compositions and the components assigned to each environment change their position toward more negative chemical shifts as the samples increase their content in Ge (Figure 7). Both facts show certainly the effect of cation distribution outside the NNN sphere (4 Å).

Ti/Ge distribution has also been analyzed in Li-$Ti_{2-x}Ge_x(PO_4)_3$ series. In order to deduce theoretical intensities of ^{31}P NMR components, the probability of finding different environments has been estimated with the expression

$$P = N \times X^n \times (1 - X)^{(4-n)}$$

where N is the number of equivalent arrangements, X and $(1 - X)$ stand for Ge and Ti molar concentrations, and n and $4 - n$ are the number of Ge and Ti in a given P environment. The calculated multiplicities of 10 detected environments follow the relation 1:(2:2):(1:2:2:1):(2:2):1 for $X = 0.5$ in agreement with NMR analysis.

In Figure 8, areas calculated with previous formula (dashed lines) and experimental values deduced from NMR spectra (detailed in section S3 of the Supporting Information) are displayed. A good agreement between calculated and experimental values is obtained confirming structural features assumed in simulations. The addition of different $Ti_{4-n}Ge_n$ intensities indicates that five chemical $P(OTi)_{4-n}(OGe)_n$ environments display intensities near the random distribution of Ti and Ge in octahedra. In this case, relative amounts of five possible environments are given by a^4, $4a^3b$, $6a^2b^2$, $4ab^3$, and b^4 values, where a and b stand for the octahedra occupation by Ti and Ge atoms. This analysis confirms again that Ge and Ti do not display any preference for two different octahedral sites, and observed features have a local origin. The absence of a periodic pattern for Ti,Ge distribution is responsible for the average $R\bar{3}c$ symmetry deduced by XRD in all members of the series.

Structural Features That Affect P Chemical Shifts. In NASICON compounds, each tetrahedron shares two O1 oxygen atoms with two octahedra of the same structural unit and two O2 oxygens of external units. Differences detected by XRD and NMR are based on the sensitivity of these two techniques to Ge for Ti substitution. All tetrahedra are equivalent in $R\bar{3}c$ S.G.; from this fact, only one site was detected in structural refinements. However, the Ge for Ti substitution produced the local differentiation of inner and outer octahedra that share O1 and O2 oxygen atoms with P tetrahedra in DFT models. This produces the splittings observed in ^{31}P NMR spectra.

DFT simulations aid us to understand the influence of different structural factors on ^{31}P chemical shifts. The analysis of P−O distances shows that P−O2 distances increase (0.008 Å) and P−O1 distances decrease (0.012 Å) with Ge/Ti substitution. The variation of R−O distances is considerable higher (0.06 Å) with Ge/Ti substitution. In Figure 9, it is observed that chemical shift of P atoms becomes more negative when the mean R−O distance decreases; however, the correlation displays a significant dispersion. In particular, chemical shifts of environments involving two Ge at both R1

DOI: 10.1021/jacs.6b03583
J. Am. Chem. Soc. 2016, 138, 9479−9486

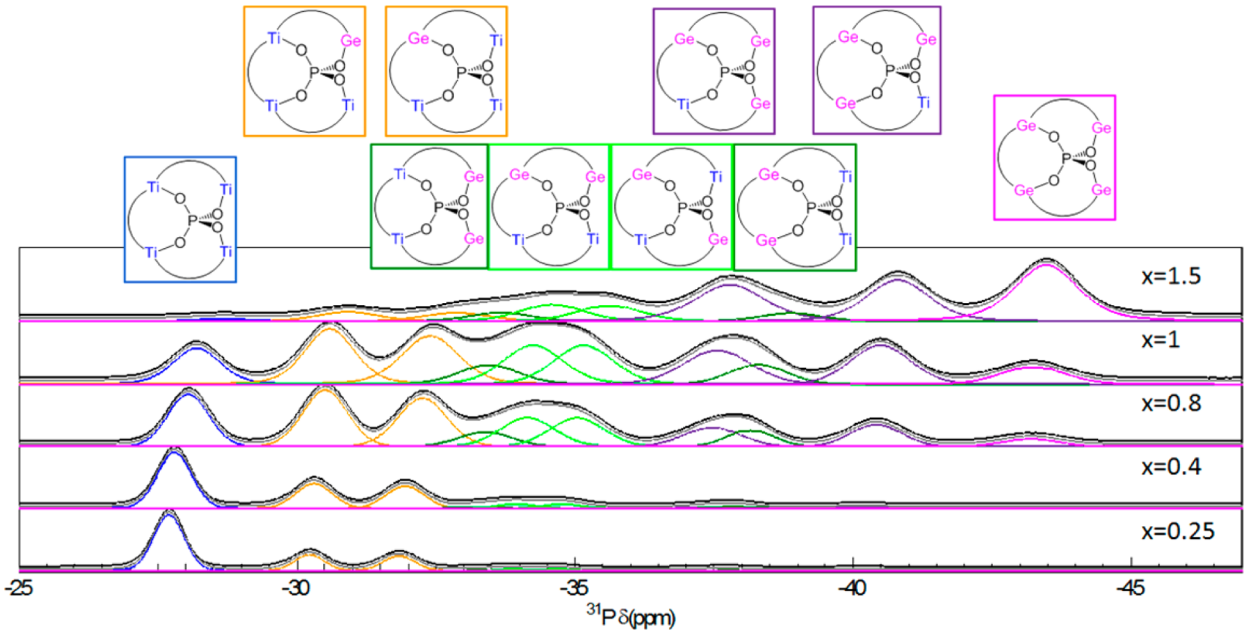

Figure 7. Deconvolution of ^{31}P MAS NMR spectra of the $LiTi_{2-x}Ge_x(PO_4)_3$ series. The assignment of components corresponds to that provided in section S3 of the Supporting Information.

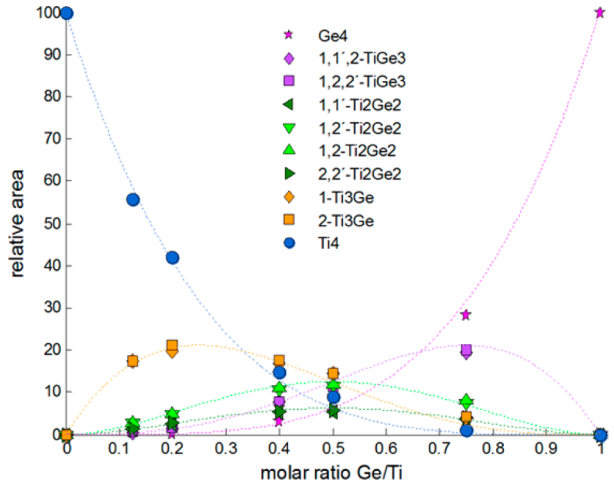

Figure 8. Experimental (symbols) and theoretical (dashed lines) areas of different ^{31}P components as a function of the molar Ge/Ti ratio.

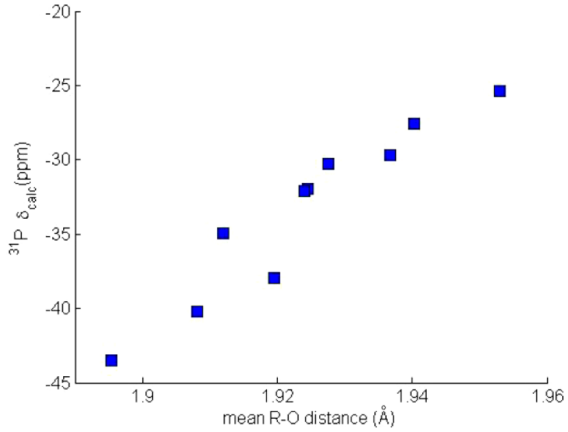

Figure 9. Dependence of ^{31}P chemical shift on average R−O distances.

and R1′ sites are shifted toward more negative values than the main observed trend, indicating that other effects apart from R−O distance must be considered.

O−P−O angles also affect ^{31}P chemical shift values. O1−P−O1 angles involving O atoms of the same lantern tend to augment from 109.3 (Ti pure phase) to 114.3 (Ge pure phase) when Ge increases; however, O1−P−O2 angles involving inner and outer oxygen atoms tend to diminish. O1−R−O1 angles augment from 93.6 in Ti to 95.1 in the Ge phase; this variation is smaller in O2−R−O2 angles. In which concern, the difference between two O1−R−O2 angles in the Ti phase (88.1 and 94.6) is slightly higher than that in the Ge phase (88.8 and 92.8), indicating a bigger twist in two parallel O planes of octahedra. Finally, mean P−O1−R angles involving O and R in positions 1 or 1′ decrease 4° from Ti to Ge end members; however, P−O2−R angles suffer a much smaller variation. From analysis of chemical shift vs angular values, the absence of a clear dependence between both parameters can be concluded.

When Ti is substituted by Ge, the charge of oxygen atoms should be modified, affecting ^{31}P chemical shifts. To better analyze the chemical shift dependence of P atoms on O charges, two oxygen types, O1 and O2, have been differentiated. DFT calculations showed that changes produced along the series in O1 Mulliken charges, from −0.90 to −1.01 (Figure 10), are bigger than those in O2 atoms, from −0.96 to −1.02 (not shown). According to this, the ^{31}P MAS NMR chemical shift dependence detected on O1 charges should be bigger than that based on O2 oxygen atoms. In Figure 10, it is shown that chemical shift values are grouped around three mean O1 charge values. The P atoms with the more negative chemical shifts of each group are linked to O2 atoms with mean charges around −1.02, while the P atoms with less negative chemical shifts are linked to O2 atoms with mean charges around −0.96. From the observed values, it can be again concluded that the Ge for Ti substitution in 1 or 1′ sites causes a bigger change on ^{31}P NMR chemical shifts than the substitution in 2 or 2′ sites.

DOI: 10.1021/jacs.6b03583
J. Am. Chem. Soc. 2016, 138, 9479−9486

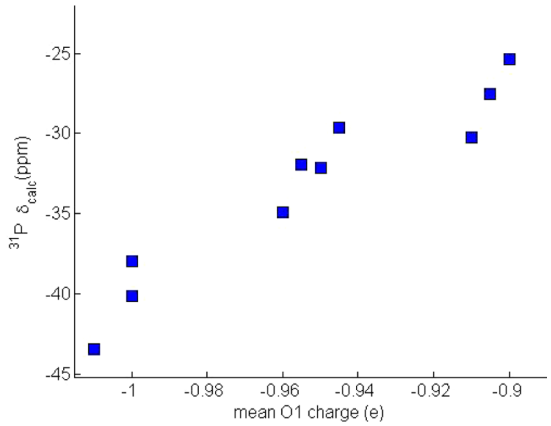

Figure 10. Dependence of ^{31}P chemical shift on individualized O1 charges.

Finally, changes produced in oxygen charges when Ti is substituted by Ge must also affect Li−O bonds, which should change Li mobility in $LiTi_{2-x}Ge_x(PO_4)_3$ series. DFT simulations were addressed to investigate interaction of lithium with oxygen atoms. In particular, changes produced on the Li charge have been analyzed. The Li Mulliken charge changes from +1.02 to +0.92 when all Ti is substituted by Ge. On the basis of this observation, it can be concluded that the higher the Li charge, the lower the covalence degree in Li−O2 bonds. According to that, Li mobility should be higher in Ti than in Ge phases, which is experimentally confirmed.[49]

CONCLUSIONS

The solid solution $LiTi_{2-x}Ge_x(PO_4)_3$ was investigated by ^{31}P NMR spectroscopy and first-principles DFT calculations. The symmetry deduced from XRD patterns is rhombohedral $R\bar{3}c$, but ^{31}P MAS NMR spectra suggest lower local symmetries for intermediate compositions.

The DFT technique has permitted the study of local disorder in long-term ordered systems. The use of lower symmetry allows the local investigation of different Ti/Ge arrangements but increases the computational cost. The strategy followed here to perform DFT calculations was to split the problem into several simple ones, preserving the symmetry as high as possible taking into account the S.G. obtained in structural refinements. To allow different cation substitutions, only some symmetry elements were eliminated. Specifically, seven $R3$ models were used to describe different Ti/Ge arrangements.

Simulation of the $LiTi_{2-x}Ge_x(PO_4)_3$ series suggests that detection of 10 P environments is mainly due to the existence of two oxygen types, O1 and O2, whose charges are differently affected by Ge and Ti occupation of octahedra. On this basis, detected bands display a multiplicity pattern 1:(2:2):(1:2:2:1):(2:2):1 that differs from 1:4:6:4:1 expected for $R\bar{3}c$ symmetry where four octahedral sites are equivalent. Monosubstituted models differentiate R1 from R2, and disubstitution generates an additional differentiation between R sites of the same type. The splitted $Ti_{4-n}Ge_n$ components display intensities that agree with the random occupation of octahedral sites by Ge and Ti cations.

ASSOCIATED CONTENT

Supporting Information

The Supporting Information is available free of charge on the ACS Publications website at DOI: 10.1021/jacs.6b03583.

Linear regression for referencing ^{31}P chemical shieldings deduced from four reported magnesium phosphates with different degrees of condensation; description of P environments contained in model TiGe3; calculated and experimental ^{31}P MAS NMR chemical shifts for $LiTi_{2-x}Ge_x(PO_4)_3$ components (PDF)

AUTHOR INFORMATION

Corresponding Author

*virginia.diez@icmm.csic.es

Present Address

†K.A.: Section of Materials & Environment, Faculty of Civil Engineering and Geosciences, Delft University of Technology, The Netherlands.

Notes

The authors declare no competing financial interest.

ACKNOWLEDGMENTS

This work has been funded by the Spanish projects MINECO MAT2013-46452-C4-2R and MATERYENER3-CAM (S2013/MIT-2753).

REFERENCES

(1) Tarascon, J. M.; Armand, M. *Nature* **2001**, *414*, 359.
(2) Knauth, P. *Solid State Ionics* **2009**, *180*, 911.
(3) Aono, H.; Imanaka, N.; Adachi, G. *Acc. Chem. Res.* **1994**, *27*, 265.
(4) Sebastian, L.; Gopalakrishnan, J. *J. Mater. Chem.* **2003**, *13*, 433.
(5) Alpen, U. V.; Rabenau, A.; Talat, G. H. *Appl. Phys. Lett.* **1977**, *30*, 621.
(6) Rodger, A. R.; Kuwano, J.; West, A. R. *Solid State Ionics* **1985**, *15*, 185.
(7) Bates, J. B.; Dudney, N. J.; Gruzalski, G. R.; Zuhr, R. A.; Choudhury, A.; Luck, C. F.; Robertson, J. D. *Solid State Ionics* **1992**, *53*, 647.
(8) Kondo, S.; Takada, K.; Yamamura, Y. *Solid State Ionics* **1992**, *53*−*56*, 1183.
(9) Adachi, G. Y.; Imanaka, N.; Aono, H. *Adv. Mater.* **1996**, *8*, 127.
(10) Stramare, S.; Thangadurai, V.; Weppner, W. *Chem. Mater.* **2003**, *15*, 3974.
(11) Thangadurai, V.; Shukla, A. K.; Gopalakrishnan, J. *J. Mater. Chem.* **1999**, *9*, 739.
(12) Sugantha, M.; Varadaraju, U. V. *Solid State Ionics* **1997**, *95*, 201.
(13) Leo, C. J.; Rao, G. V. S.; Chowdari, B. V. R. *J. Mater. Chem.* **2002**, *12*, 1848.
(14) Alami, M.; Brochu, R.; Soubeyroux, J. L.; Gravereau, P.; Leflem, G.; Hagenmuller, P. *J. Solid State Chem.* **1991**, *90*, 185.
(15) Qui, D. T.; Hamdoune, S.; Soubeyroux, J. L.; Prince, E. *J. Solid State Chem.* **1988**, *72*, 309.
(16) Morin, E.; Angenault, J.; Couturier, J. C.; Quarton, M.; He, H.; Klinowski, J. *Eur. J. Solid State Inorg. Chem.* **1997**, *34*, 947.
(17) Losilla, E. R.; Aranda, M. A. G.; MartinezLara, M.; Bruque, S. *Chem. Mater.* **1997**, *9*, 1678.
(18) Catti, M.; Stramare, S.; Ibberson, R. *Solid State Ionics* **1999**, *123*, 173.
(19) Goodenough, J. B.; Hong, H. Y. P.; Kafalas, J. A. *Mater. Res. Bull.* **1976**, *11*, 203.
(20) Hamdoune, S.; Qui, D. T.; Schouler, E. J. L. *Solid State Ionics* **1986**, *18*−*19*, 587.
(21) Arbi, K.; Mandal, S.; Rojo, J. M.; Sanz, J. *Chem. Mater.* **2002**, *14*, 1091.
(22) Huang, L.; Wen, Z.; Wu, M.; Wu, X.; Liu, Y.; Wang, X. *J. Power Sources* **2011**, *196*, 6943.
(23) Mariappan, C. R.; Gellert, M.; Yada, C.; Rosciano, F.; Roling, B. *Electrochem. Commun.* **2012**, *14*, 25.
(24) Arbi, K.; Hoelzel, M.; Kuhn, A.; Garcia-Alvarado, F.; Sanz, J. *Inorg. Chem.* **2013**, *52*, 9290.

DOI: 10.1021/jacs.6b03583
J. Am. Chem. Soc. 2016, 138, 9479−9486

(25) Clement, R. J.; Pell, A. J.; Middlemiss, D. S.; Strobridge, F. C.; Miller, J. K.; Whittingham, M. S.; Emsley, L.; Grey, C. P.; Pintacuda, G. *J. Am. Chem. Soc.* **2012**, *134*, 17178.
(26) Charpentier, T. *Solid State Nucl. Magn. Reson.* **2011**, *40*, 1.
(27) Bonhomme, C.; Gervais, C.; Babonneau, F.; Coelho, C.; Pourpoint, F.; Azaïs, T.; Ashbrook, S. E.; Griffin, J. M.; Yates, J. R.; Mauri, F.; Pickard, C. J. *Chem. Rev.* **2012**, *112*, 5733.
(28) Winkler, B.; Hytha, M.; Pickard, C.; Milman, V.; Warren, M.; Segall, M. *Eur. J. Mineral.* **2001**, *13*, 343.
(29) Winkler, B.; Pickard, C. J.; Segall, M. D.; Milman, V. *Phys. Rev. B: Condens. Matter Mater. Phys.* **2001**, *63*, 214103.
(30) Sene, S.; Bouchevreau, B.; Martineau, C.; Gervais, C.; Bonhomme, C.; Gaveau, P.; Mauri, F.; Begu, S.; Mutin, P. H.; Smith, M. E.; Laurencin, D. *CrystEngComm* **2013**, *15*, 8763.
(31) Gervais, C.; Coelho, C.; Azaïs, T.; Maquet, J.; Laurent, G.; Pourpoint, F.; Bonhomme, C.; Florian, P.; Alonso, B.; Guerrero, G.; Mutin, P. H.; Mauri, F. *J. Magn. Reson.* **2007**, *187*, 131.
(32) Gervais, C.; Profeta, M.; Lafond, V.; Bonhomme, C.; Azais, T.; Mutin, H.; Pickard, C. J.; Mauri, F.; Babonneau, F. *Magn. Reson. Chem.* **2004**, *42*, 445.
(33) Arbi, K.; Ayadi-Trabelsi, M.; Sanz, J. *J. Mater. Chem.* **2002**, *12*, 2985.
(34) Rodriguez-Carvajal, J. *Phys. B* **1993**, *192*, 55.
(35) Massiot, D.; Fayon, F.; Capron, M.; King, I.; Le Calvé, S.; Alonso, B.; Durand, J.-O.; Bujoli, B.; Gan, Z.; Hoatson, G. *Magn. Reson. Chem.* **2002**, *40*, 70.
(36) Clark, S. J.; Segall, M. D.; Pickard, C. J.; Hasnip, P. J.; Probert, M. J.; Refson, K.; Payne, M. C. *Z. Kristallogr. - Cryst. Mater.* **2005**, *220*, 567.
(37) Pickard, C. J.; Mauri, F. *Phys. Rev. B: Condens. Matter Mater. Phys.* **2001**, *63*, 245101.
(38) Perdew, J. P.; Burke, K.; Ernzerhof, M. *Phys. Rev. Lett.* **1996**, *77*, 3865.
(39) Yates, J. R.; Pickard, C. J.; Mauri, F. *Phys. Rev. B: Condens. Matter Mater. Phys.* **2007**, *76*, 024401.
(40) Aatiq, A.; Menetrier, M.; Croguennec, L.; Suard, E.; Delmas, C. *J. Mater. Chem.* **2002**, *12*, 2971.
(41) Vegard, L. *Eur. Phys. J. A* **1921**, *5*, 17.
(42) Yue, Y.; Deng, F.; Hu, H.; Ye, C.; Lin, Z.; Tian, S. *Chem. Phys. Lett.* **1993**, *208*, 311.
(43) Colmont, M.; Delevoye, L.; Ketatni, E. M.; Montagne, L.; Mentré, O. *J. Solid State Chem.* **2006**, *179*, 2111.
(44) Kulshreshtha, S. K.; Jayakumar, O. D.; Sudarsan, V. *J. Solid State Chem.* **2010**, *183*, 1071.
(45) Losilla, E. R.; Aranda, M. A. G.; Bruque, S.; Sanz, J.; Paris, M. A.; Campo, J.; West, A. R. *Chem. Mater.* **2000**, *12*, 2134.
(46) Reader, S. W.; Mitchell, M. R.; Johnston, K. E.; Pickard, C. J.; Whittle, K. R.; Ashbrook, S. E. *J. Phys. Chem. C* **2009**, *113*, 18874.
(47) Mitchell, M. R.; Reader, S. W.; Johnston, K. E.; Pickard, C. J.; Whittle, K. R.; Ashbrook, S. E. *Phys. Chem. Chem. Phys.* **2011**, *13*, 488.
(48) Griffin, J. M.; Yates, J. R.; Berry, A. J.; Wimperis, S.; Ashbrook, S. E. *J. Am. Chem. Soc.* **2010**, *132*, 15651.
(49) Martinez-Juarez, A.; Pecharroman, C.; Iglesias, J. E.; Rojo, J. M. *J. Phys. Chem. B* **1998**, *102*, 372.

DOI: 10.1021/jacs.6b03583
J. Am. Chem. Soc. 2016, 138, 9479−9486